The Planckian Distribution Equation As A Novel Method To Predict The Efficacy Of Breast

Cancer Pharmacotherapy

Shreshth Rajan

Manalapan High School Science & Engineering Academy

422srajan@frhsd.com

+1 848-482-0204

**Abstract**:

Chemotherapy-related deaths, the result of treatment with faulty medications, account for nearly 10% of all breast cancer deaths (Rashbass, 2016). Patient-specific, personalized medicine is evidently required to administer optimized therapeutics and prevent treatment-related mortality. In order to develop a predictive model for breast cancer therapy, the following study analyzed the mRNA data of 4,704 genes derived from 20 breast cancer patients before and after doxorubicin treatment for 16 weeks (O'brien et al., 2006; Perou et al., 2000). The genomic data of each patient was first stratified into 9 groups (corresponding to the 9 Mechanisms defined in Figure 4) based on mRNA expression in response to the tumor and to the doxorubicin treatment. The study then employed the Planckian Distribution Equation (PDE) discovered at Rutgers University to model the stratified samples by transforming each mechanism into a single long-tailed histogram fitted by the PDE. Our PDE model is based on 3 parameters - A, B, and C - of which 2 were extracted from each model to generate the plots seen in figures 5e and 5f. The drug-induced slopes of the A vs C plots were then determined for all 9 mechanisms of each patient. The study observed an increase in post-treatment mRNA levels for longer surviving patients in 6 mechanisms. Further analysis displayed how the drug treatment uniquely altered each of the mechanisms based on the length of patient survival. These results indicate that the PDE-based procedures described herein may provide a novel tool for discovering potential anti-breast cancer pharmaceuticals.


*Keywords:* Planckian Distribution Equation, breast cancer, mRNA, chemotherapy.

## Introduction:

Treatment for breast cancer has evolved from mid-19th century radical mastectomy to Sidney Farber's antifolate revolution and now to an optimized multi-pronged combination of chemotherapy and surgery. Despite these advancements, breast carcinoma has remained an extremely fatal malignancy, killing an estimated 42,170 females in 2019, the second most of any cancer ("Top 5 Most Dangerous Cancers," 2020). Thus, as the days of radical mastectomy as an optimal treatment method wane in the distant past, the need for patient-specific personalized chemotherapy only becomes more significant. Clinical studies have estimated that nearly 7.5% of all cancer deaths are caused by chemotherapy -- over-treatment with faulty medications (Rashbass, 2016). A dire need for advanced research into pre-determining the effectiveness of breast cancer pharmacotherapy exists, with the livelihood of millions of women at stake. The following paper provides a novel method for predicting the clinical success of anti-breast cancer drugs based on the Planckian Distribution Equation (PDE).

In 2000, Perou et al. (2000) at Stanford University measured the RNA levels of 8,102 genes in breast cancer tissues biopsied from patients before and after 16-week doxorubicin treatment using Microarray techniques. Our study removed those genes whose RNA data were not complete, leaving a total 4,740 select open reading frames (ORFs) per patient. From each patient, two groups of data were designated as $\Delta T$ and $\Delta D$, depending on the magnitude of RNA changes are due to tumor (T) or due to drug (D) treatment respectively. The pair of $\Delta T$ and $\Delta D$ values were converted into an angle using the formula $\alpha = \arctan(\Delta D/\Delta T)$, which creates the following 9 classes - mechanisms - of angles: 1(-22.5 - 22.5), 2(22.6 - 67.5), 3(67.6 - 112.5), etc. (see **Figure 4**).  Our study then analyzed each mRNA mechanism to determine if a significant difference existed between long-surviving and short-surviving patients.

The results detected a statistically greater change in the slope of the A vs. C plots of PDE, in which the x coordinates represent $\log(A*10^3)$ and the y coordinate represents the C parameter, for long surviving patients compared to short surviving patients. These results indicate that doxorubicin-induced changes were greater among long surviving patients than short surviving patients. Since the analysis is based on individual patient data, these novel results, if mimicked by other anti-cancer therapy candidates, can be utilized to discover the most effective cancer pharmaceuticals for treating individual patients. The following section details the microarray data collection methodology for each breast cancer patient. It then outlines the theoretical background of the Planckian Distribution Equation algorithm and its application to cancer pharmacotherapy. The application of the PDE is then described more specifically for our breast cancer transcriptome.

## Materials and Methods:

The project was conducted completely virtually, with the aforementioned microarray data collection having been included in Perou et., al 2000. All statistical methods and algorithms were employed via machine learning tools such as Microsoft Excel.

**Microarray data collection and analysis:**

DNA Microarray data collection is among the most significant tools utilized for thorough understanding of functional genomics (Grigoryev et al., 2020). This study equipped advanced use of microarray analysis to extract key data from biopsied tumor tissue before and after doxorubicin treatment.

Micoarray experimentation occurs as a result of excess cellular mRNA degradation and transcription. Expressed genes are transcribed into mRNA, which are isolated and converted into complementary strands of cDNA via the enzyme reverse transcriptase. **Figure 1** displays how

the mRNA levels inside the cell are affected by the two opposing processes – (i) increases in the rate of transcription of mRNA to cDNA catalyzed by transcriptome and (ii) transcript degradation of excess mRNA catalyzed by degradosome.
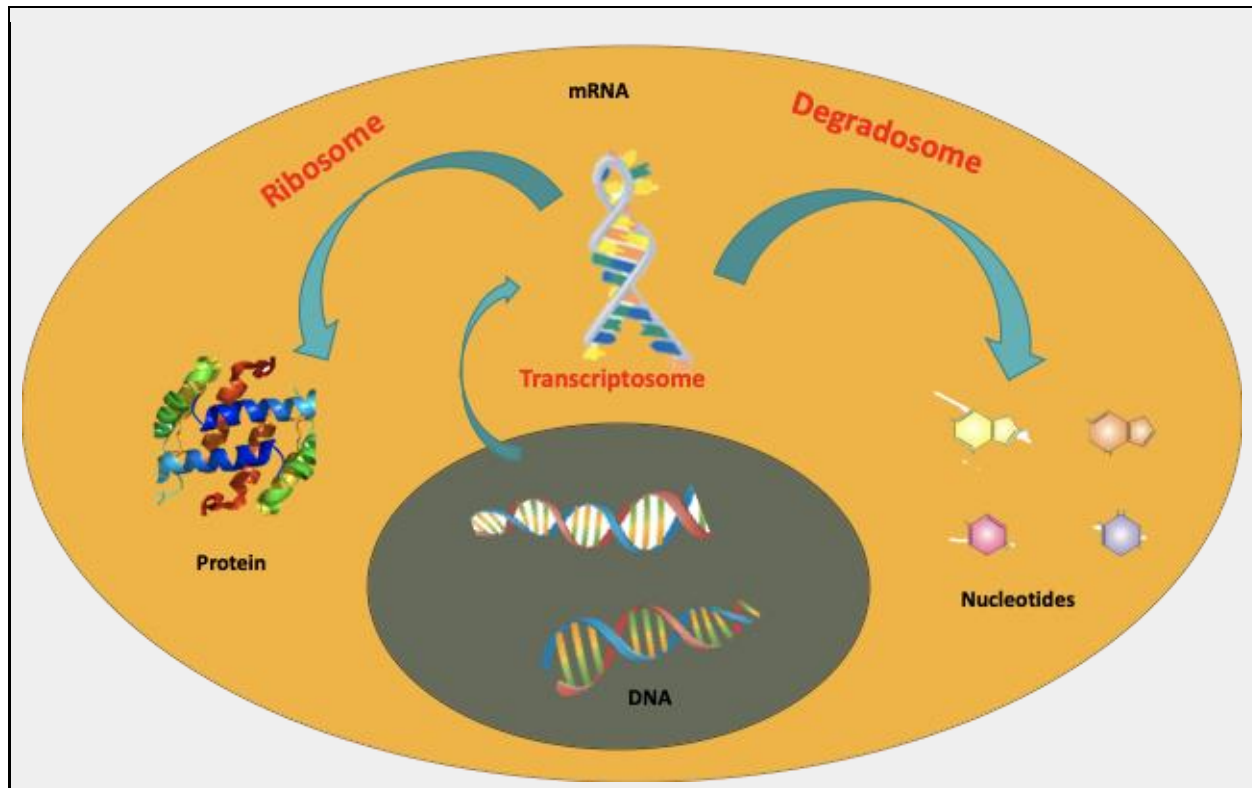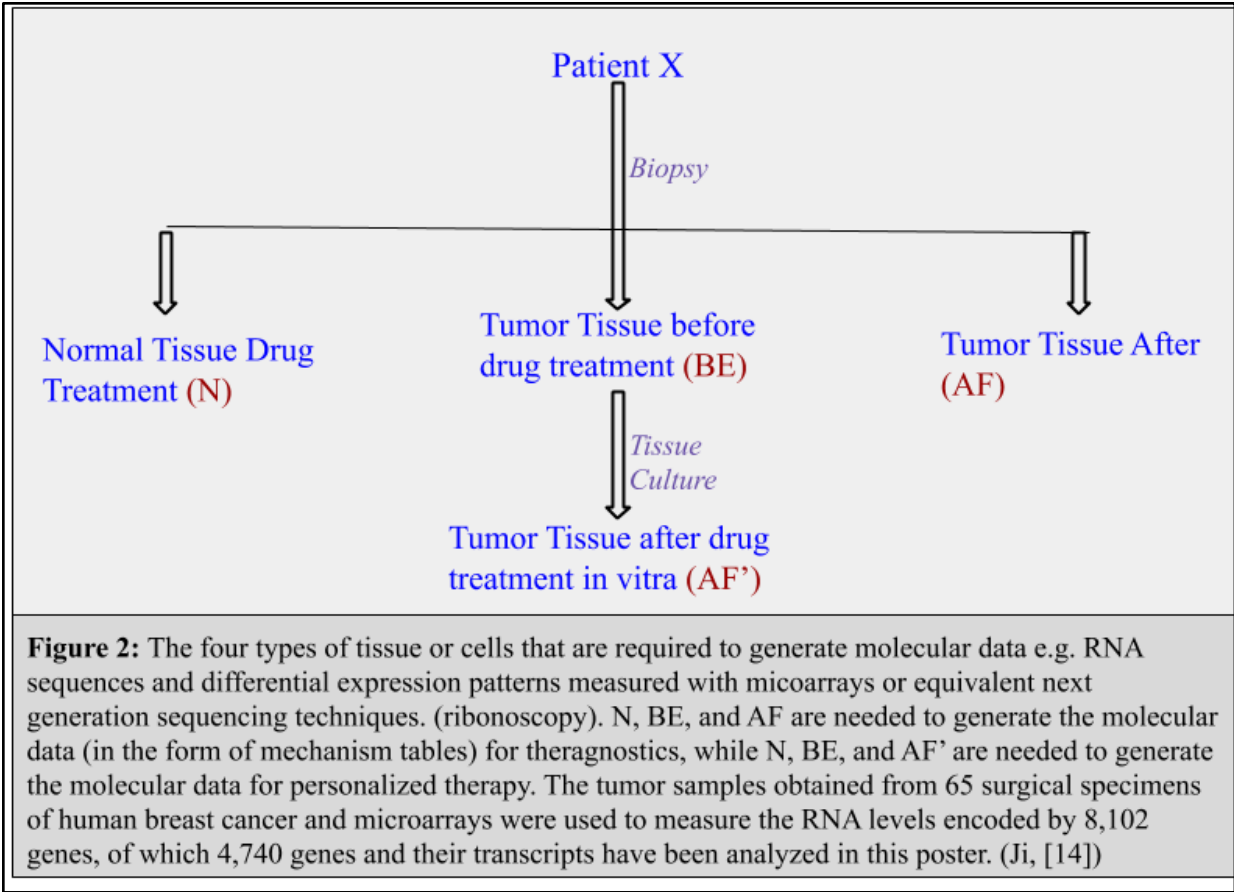


**Figure 1:** The conversion of DNA to mRNA and protein via the enzyme transcriptase and ribosomes. The figure also displays the process by which mRNA molecules are degraded to nucleotides for recycling. Two routes by which  mRNA levels can be affected are (i) changes in the rate of transcription of DNA to mRNAby transcriptosome, and (ii) changes in rate of degradation of mRNA into nucleotide by degradosome
(Kim, Chaewon *Breast Cancer and PDE,* 2018)

The microarray experiments involved the following 6 key steps to effectively measure mRNA levels within cells: (1) Isolate RNAs from broken cells. (2) Synthesize fluorescently labeled cDNA from isolated RNAs using reverse transcriptase and appropriately fluorescently labeled nucleotides. (3) Prepare a microarray either with EST (expressed sequence tag, i.e sequences several hundred nucleotides long that are complementary to the stretches of the genome encoding RNAs) or oligonucleotides (synthesized right on the microarray surface). (4)

Pour the fluorescently labeled cDNA preparation over the microarray surface to effect

hybridization and wash off excess debris. (5) Measure the light intensity of fluorescently labeled

cDNA bound to the microarray surface using a computer-assisted microscope. (6) Display the

final result as a table of numbers, each registering the fluorescent intensity of a square on the

microarray which is proportional to the concentration of cDNA (and ultimately to the RNA

levels in cells before isolation) located at row x and column y, rows indicating the identity of

genes, and y the time or the conditions under which the RNA levels are measured (Ji, 2012; Ji,

2012).

From each patient, the molecular data from 4 distinct tissue and cell types were generated

as shown in **Figure 2**. Treatment groups normal tissue (N), before treatment (BE), and after

treatment (AF) generated the molecular data (in the form of the mechanism tables seen in **Figure

4**) for the study into theranostics and personalized therapy (Ji 2012). Microarray analysis was

then used to measure RNA sequences and differential expression patterns among data groups - a

process collectively known as ribonoscopy (Ji 2012). The tumor samples were used to measure

RNA levels encoded by a total of 8,102 genes, of which 4,740 genes and their transcripts have

been analyzed here. **Figure 3** displays a partial list of the microarray data measured from the

normal breast cancer cell culture (N) and the breast cancer tissues of patients #7, #27, and #39

measured before (BE) and after (AF) doxorubicin treatment for 16 weeks.

**Figure 2:** The four types of tissue or cells that are required to generate molecular data e.g. RNA sequences and differential expression patterns measured with micoarrays or equivalent next generation sequencing techniques. (ribonoscopy). N, BE, and AF are needed to generate the molecular data (in the form of mechanism tables) for theragnostics, while N, BE, and AF' are needed to generate the molecular data for personalized therapy. The tumor samples obtained from 65 surgical specimens of human breast cancer and microarrays were used to measure the RNA levels encoded by 8,102 genes, of which 4,740 genes and their transcripts have been analyzed in this poster. (Ji, [14])

| ORF | Norma l 1 | Norma l 2 | Norma l 3 | Avg(N) | 7-Before | 7-AF | 27-BE | 27-AF | 39-BE | 39-AF |
|-----|-----------|-----------|-----------|--------|----------|------|-------|-------|-------|-------|
| ACACB | 0.568 | 4.493 | 4.790 | 3.284 | 0.851 | 5.473 | 1.131 | 1.044 | 0.881 | 1.107 |
| ACTC | 1.441 | 1.036 | 0.417 | 0.964 | 0.762 | 0.936 | 0.583 | 0.585 | 0.774 | 0.650 |
| ATF2 | 0.800 | 1.131 | 0.566 | 0.832 | 0.620 | 0.660 | 0.579 | 0.691 | 0.908 | 0.690 |
| LOC51576 | 0.805 | 0.792 | 0.549 | 0.715 | 1.040 | 1.175 | 0.752 | 0.775 | 1.089 | 0.851 |
| ALB | 1.244 | 1.149 | 0.868 | 1.087 | 0.382 | 1.121 | 1.182 | 1.354 | 1.615 | 1.043 |
| AKR7A2 | 0.871 | 0.963 | 0.900 | 0.911 | 0.911 | 0.823 | 4.347 | 4.806 | 0.604 | 0.631 |
| ALPP | 1.514 | 0.920 | 0.820 | 1.084 | 0.731 | 3.134 | 0.844 | 0.950 | 1.329 | 2.136 |
| AMMECR1 | 0.961 | 1.286 | 0.446 | 0.898 | 0.478 | 0.575 | 0.525 | 0.593 | 0.607 | 0.832 |
| ABP/ZF | 7.576 | 3.142 | 2.152 | 4.290 | 0.590 | 2.988 | 0.710 | 0.887 | 5.116 | 2.066 |
| AS3 | 1.007 | 1.002 | 0.728 | 0.912 | 0.850 | 0.927 | 1.674 | 1.864 | 1.261 | 0.733 |
| ANK3 | 2.213 | 1.653 | 0.482 | 1.449 | 2.216 | 0.910 | 0.193 | 0.211 | 4.068 | 2.173 |

| | | | | | | | | | | |
|---|---|---|---|---|---|---|---|---|---|---|
| ANK3 | 1.889 | 1.902 | 0.811 | 1.534 | 2.233 | 2.010 | 0.149 | 0.216 | 3.888 | 2.834 |
| AHR | 0.605 | 0.642 | 0.815 | 0.688 | 0.998 | 1.475 | 0.288 | 0.446 | 1.165 | 0.975 |
| ATP6A1 | 0.849 | 0.803 | 0.570 | 0.741 | 0.918 | 1.295 | 1.719 | 2.040 | 0.873 | 0.575 |
| ABCF3 | 1.080 | 1.010 | 2.392 | 1.494 | 2.284 | 1.358 | 1.168 | 1.324 | 0.998 | 1.163 |
| BAGE | 0.763 | 0.628 | 1.195 | 0.862 | 0.765 | 0.831 | 0.864 | 0.878 | 0.831 | 1.030 |
| BZRP | 1.529 | 1.374 | 1.848 | 1.584 | 1.915 | 2.486 | 1.890 | 1.177 | 2.325 | 1.998 |
| BLVRB | 1.722 | 1.791 | 3.630 | 2.381 | 0.383 | 1.431 | 0.467 | 0.420 | 1.460 | 2.498 |
| CAMK2G | 0.729 | 0.822 | 0.699 | 0.750 | 0.748 | 0.853 | 1.666 | 1.552 | 0.838 | 0.667 |
| CANX | 1.059 | 1.006 | 0.451 | 0.839 | 0.916 | 0.891 | 0.536 | 0.640 | 0.492 | 0.521 |
| CRTAP | 1.185 | 1.591 | 1.347 | 1.374 | 0.773 | 1.386 | 0.531 | 0.732 | 0.759 | 1.243 |
| CTNNA1 | 0.476 | 0.497 | 0.385 | 0.453 | 0.804 | 0.926 | 0.643 | 0.644 | 0.687 | 0.610 |
| LOC56996 | 0.928 | 0.991 | 0.528 | 0.815 | 0.834 | 0.595 | 1.514 | 1.663 | 0.768 | 1.644 |
| CITED1 | 2.018 | 2.925 | 3.103 | 2.682 | 0.774 | 1.576 | 0.823 | 0.520 | 0.833 | 1.795 |
| CIDEB | 2.261 | 1.106 | 1.384 | 1.584 | 3.789 | 4.753 | 1.677 | 1.613 | 1.968 | 4.076 |
| CENPE | 0.976 | 0.744 | 0.602 | 0.774 | 1.143 | 1.405 | 0.858 | 0.890 | 1.019 | 0.707 |
| CGI-204 | 0.491 | 0.376 | 0.366 | 0.411 | 1.108 | 2.123 | 0.714 | 0.893 | 0.734 | 1.181 |
| LOC51622 | 2.711 | 1.220 | 2.863 | 2.265 | 3.654 | 2.073 | 2.676 | 1.844 | 2.075 | 3.663 |
| LOC51622 | 0.512 | 0.698 | 0.515 | 0.575 | 0.919 | 0.954 | 0.891 | 1.134 | 0.548 | 0.309 |
| CHRNE | 1.414 | 1.288 | 1.303 | 1.335 | 1.432 | 0.249 | 1.388 | 1.303 | 2.072 | 1.104 |
| CHP1 | 0.716 | 0.555 | 0.257 | 0.509 | 0.474 | 0.341 | 0.657 | 0.582 | 0.965 | 0.471 |
| C21ORF56 | 1.248 | 1.538 | 1.429 | 1.405 | 0.920 | 1.412 | 0.889 | 1.185 | 1.258 | 1.305 |
| ORF1 | 0.343 | 0.505 | 1.243 | 0.697 | 1.283 | 3.020 | 0.628 | 1.121 | 0.041 | 0.969 |
| CYP | 0.190 | 0.346 | 0.100 | 0.212 | 0.757 | 0.957 | 0.384 | 0.430 | 0.907 | 0.566 |
| CLU | 1.939 | 2.154 | 1.097 | 1.730 | 0.877 | 0.719 | 1.758 | 1.765 | 1.028 | 0.868 |
| CLU | 5.682 | 3.616 | 2.835 | 4.044 | 1.671 | 2.423 | 5.532 | 9.168 | 2.453 | 2.079 |
| CLU | 2.530 | 2.017 | 1.405 | 1.984 | 1.275 | 1.462 | 2.301 | 3.264 | 1.617 | 1.302 |
| MYCBP | 0.617 | 0.680 | 0.487 | 0.595 | 2.523 | 1.612 | 1.183 | 1.224 | 0.718 | 0.454 |
| COPB2 | 0.255 | 0.275 | 0.294 | 0.275 | 0.604 | 0.312 | 0.534 | 0.616 | 0.500 | 0.351 |
| CFL1 | 1.257 | 0.522 | 1.311 | 1.030 | 1.992 | 4.343 | 1.993 | 6.790 | 3.245 | 2.136 |

| | | | | | | | | | | |
|---|---|---|---|---|---|---|---|---|---|---|
| COL1A1 | 1.080 | 1.006 | 0.246 | 0.777 | 0.981 | 2.420 | 0.980 | 1.104 | 1.325 | 0.871 |
| COL11A1 | 0.392 | 0.401 | 1.179 | 0.657 | 3.282 | 34.870 | 7.129 | 4.118 | 24.562 | 31.278 |
| C1NH | 1.057 | 0.829 | 0.607 | 0.831 | 0.707 | 1.206 | 1.039 | 0.865 | 1.098 | 1.310 |
| C1GALT1 | 1.028 | 1.112 | 0.863 | 1.001 | 1.283 | 1.025 | 0.802 | 0.739 | 0.930 | 1.123 |
| COX11 | 0.639 | 0.719 | 0.506 | 0.621 | 0.825 | 0.618 | 1.494 | 1.601 | 0.500 | 0.408 |
| CRB1 | 1.400 | 0.819 | 0.960 | 1.060 | 1.071 | 4.684 | 1.261 | 1.512 | 2.654 | 1.651 |

**Figure 3.** A partial list of the original microarray data measured from normal breast tissues (N) and breast cancer patients #7, #27 and #39 before (BE) and after (AF) treated with doxorubicin for 16 weeks.

The mRNA changes were then classified into 9 distinct groups based on the magnitude of each change due to tumor ($\Delta T$) and due to drug treatment ($\Delta D = AF - BE$). These groups were generated based on a unit circle angle measure, where angle $\alpha° = \arctan (\Delta D/\Delta T)$ (see **figure 4a**). **Figure 4b** displays the classification method for mechanisms 1-8 based on the $\alpha$ values ($0°$ - $22.5°$, $22.5°$ - $45°$, $45°$ to $67.5°$, etc.). Mechanism 9 is classified as the range of angles excluding those lying outside the mean +/- 2 standard deviations ($\alpha = $ +/- 5%) for each other mechanism. By developing this angle that compares expression before and after treatment, the study was able to generate a single value that specifically illustrates the effectiveness of the treatment on each ORF. These 9 mechanisms provide key insights into the relationship between pretreatment tumor mRNA change and post-doxorubicin treatment change, allowing us to categorize the drug-induced changes in the tumor tissue.

| Mechanism Number | Angle (α) from the mechanism circle (°) | Effects on RNA levels due to | |
|---|---|---|---|
| | | Tumor (ΔT) | Drug (ΔD) |
| 1 | -22.5 ~ 22.5 | + | 0 |
| 2 | 22.6 ~ 67.5 | + | + |
| 3 | 67.6 ~ 112.5 | 0 | + |
| 4 | 112.6 ~ 157.5 | - | + |
| 5 | 157.6 ~ 202.5 | - | 0 |
| 6 | 202.6 ~ 249.5 | - | - |
| 7 | 249.6 ~ 292.5 | 0 | - |
| 8 | 292.6 ~ -22.5 | + | - |
| 9 | Defined as the mean +/- 5% of the range of angles excluding those lying outside of the mean +/- 2 σ's. | 0 | 0 |
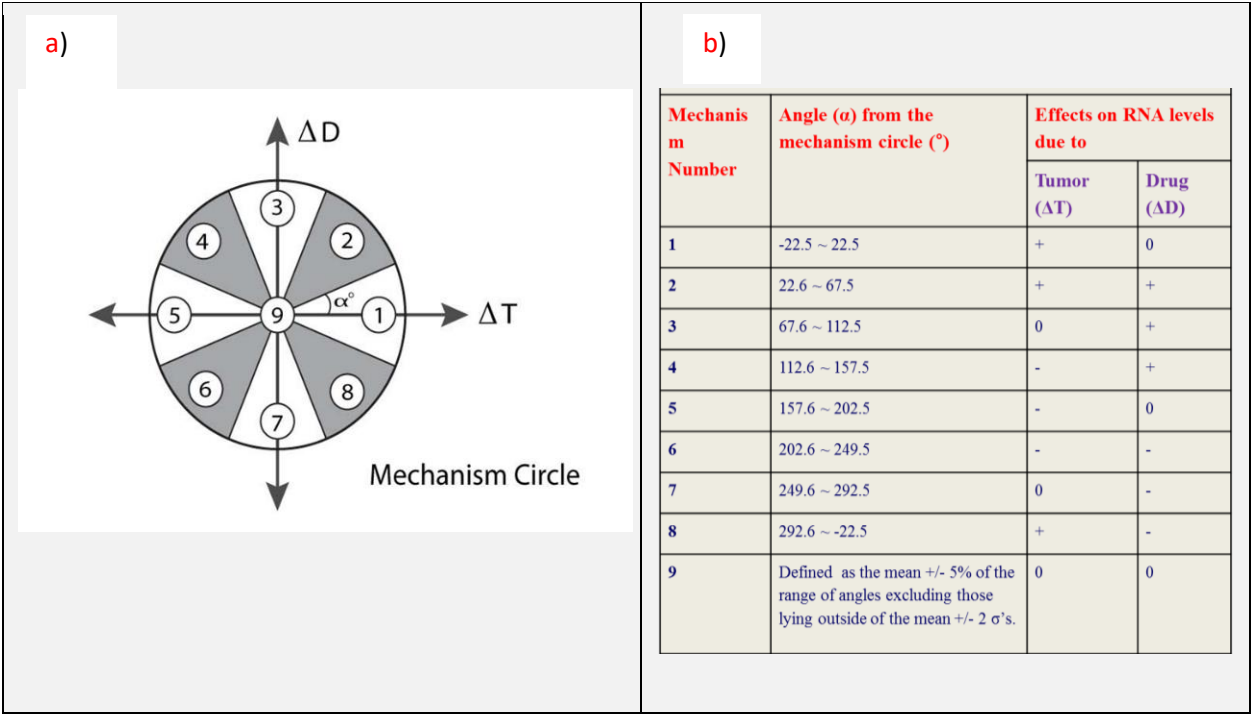
**Figure 4.** The mechanism circle.
 ΔT = Change in RNA levels due to tumor, i.e., BE-N in Panel a) **A**; ΔD = Change in RNA levels in tumor tissues due to drug treatment, i.e., A – BE.  The angle α was measured counterclockwise starting from the positive x-axis as α = arctan (ΔD/ ΔT). Each of the 9 mechanisms is defined in terms of the range of the associated α values as indicated in Panel b). The angle for Mechanism 9 cannot be so calculated.

The results of the microarray analysis are displayed in a tabular form exemplified by

**Table 1,** in which N = the number of patients; n= the number of ORF (open-reading frames of

single genes), SM = patient survival period in months, N = normal tissue biopsies, BE = pre-drug

treated tissue, AF = post-drug treated tissue, and M = the mechanism number as defined in

**Figure 4**.  **Table 2** displays an extracted portion of the mechanism summary table, which

quantified each ORF in each of the 20 patients as one of the 9 mechanisms. The microarray

analysis provided a thorough method to classify each of 20 doxorubicin-treated breast cancer

patients by genome, allowing us to create a patient-specific methodology for treatment efficacy.

| ORF | Patient 1 | | | | Patient 2 | | | | . . . | Patient N | | | |
|---|---|---|---|---|---|---|---|---|---|---|---|---|---|
| | N | BE | AF | **M** | N | BE | AF | **M** | **. . .** | N | BE | AF | **M** |

| 1 | | | | 2 | | | | 1 | ... | | | | 6 |
|---|---|---|---|---|---|---|---|---|---|---|---|---|---|
| 2 | | | | 3 | | | | 6 | ... | | | | 2 |
| 3 | | | | 8 | | | | 5 | ... | | | | 7 |
| 4 | | | | 1 | | | | 4 | ... | | | | 9 |
| ... | | | | ... | | | | ... | ... | | | | ... |
| n | | | | 5 | | | | 6 | ... | | | | 1 |

**Table 1.** The structure of the microarray data measured from 20 breast cancer patients before (BE) and after (AF) treatment with doxorubicin for 16 weeks. ORF = Open reading frame; N = normal human breast tissue; BE = before treatment; AF = after treatment; M = Mechanism. N = the number of the ORF analyzed; N = the number of patients.

| ORF | Symbol | P1 | P2 | P3 | P4 | P5 | P6 | P7 | P8 | P9 | P10 | P11 | P12 | P13 | P14 | P15 | P16 | P17 | P18 | P19 | P20 |
|---|---|---|---|---|---|---|---|---|---|---|---|---|---|---|---|---|---|---|---|---|---|
| 1 | ZFX | 9 | 8 | 2 | 8 | 3 | 2 | 2 | 2 | 8 | 4 | 9 | 5 | 8 | 9 | 1 | 1 | 9 | 8 | 2 | 1 |
| 2 | CDC34 | 9 | 9 | 4 | 8 | 9 | 8 | 7 | 1 | 8 | 2 | 8 | 5 | 9 | 8 | 2 | 8 | 9 | 1 | 3 | 9 |
| 3 | UQCRH | 9 | 8 | 2 | 8 | 7 | 8 | 8 | 9 | 9 | 2 | 1 | 5 | 8 | 8 | 2 | 8 | 3 | 8 | 1 | 1 |
| 4 | TIMP1 | 8 | 9 | 3 | 9 | 8 | 9 | 1 | 9 | 9 | 1 | 9 | 5 | 9 | 1 | 9 | 9 | 8 | 9 | 1 | 9 |
| 5 | RELA | 9 | 1 | 9 | 8 | 9 | 1 | 8 | 8 | 8 | 3 | 9 | 5 | 9 | 8 | 3 | 8 | 4 | 2 | 3 | 9 |
| 6 | ACAT2 | 8 | 9 | 4 | 9 | 8 | 8 | 8 | 1 | 8 | 9 | 8 | 5 | 9 | 9 | 9 | 9 | 7 | 9 | 9 | 9 |
| 7 | TRA@ | 8 | 2 | 8 | 3 | 3 | 1 | 8 | 8 | 1 | 1 | 1 | 7 | 8 | 8 | 1 | 1 | 1 | 1 | 3 | 1 |
| 8 | RBM5 | 7 | 1 | 4 | 8 | 9 | 2 | 7 | 1 | 8 | 4 | 8 | 5 | 6 | 7 | 2 | 7 | 4 | 8 | 3 | 1 |
| 9 | SFRS10 | 8 | 9 | 3 | 8 | 8 | 9 | 9 | 1 | 8 | 9 | 9 | 5 | 9 | 8 | 2 | 9 | 8 | 8 | 9 | 9 |
| 10 | RBM3 | 1 | 2 | 2 | 8 | 8 | 2 | 1 | 1 | 8 | 3 | 2 | 3 | 9 | 8 | 2 | 8 | 1 | 1 | 2 | 9 |
| 11 | PXN | 9 | 7 | 3 | 7 | 9 | 5 | 4 | 7 | 5 | 4 | 4 | 5 | 8 | 7 | 3 | 9 | 5 | 5 | 5 | 6 |
| 12 | TM9SF2 | 1 | 9 | 8 | 1 | 1 | 1 | 1 | 1 | 8 | 1 | 8 | 8 | 8 | 1 | 2 | 3 | 8 | 1 | 1 | 9 |
| 13 | MLF2 | 8 | 1 | 1 | 8 | 8 | 1 | 8 | 1 | 9 | 1 | 8 | 5 | 8 | 9 | 2 | 9 | 8 | 9 | 1 | 2 |
| 14 | ABCC5 | 8 | 1 | 1 | 9 | 1 | 2 | 1 | 1 | 8 | 2 | 2 | 5 | 1 | 2 | 2 | 1 | 8 | 1 | 2 | 2 |
| 15 | DECR1 | 1 | 3 | 4 | 8 | 8 | 1 | 1 | 1 | 8 | 2 | 3 | 3 | 8 | 9 | 2 | 3 | 8 | 8 | 2 | 3 |
| 16 | LOC55977 | 8 | 2 | 1 | 8 | 9 | 9 | 1 | 1 | 8 | 3 | 8 | 5 | 1 | 8 | 9 | 9 | 1 | 8 | 2 | 1 |
| 17 | PPFIA1 | 1 | 2 | 2 | 8 | 8 | 1 | 1 | 1 | 8 | 3 | 1 | 4 | 8 | 1 | 2 | 8 | 1 | 1 | 2 | 1 |
| 18 | ELAVL1 | 9 | 9 | 3 | 8 | 8 | 9 | 9 | 1 | 8 | 2 | 8 | 5 | 8 | 8 | 2 | 8 | 9 | 8 | 2 | 9 |
| 19 | RBM4 | 8 | 2 | 2 | 8 | 1 | 2 | 1 | 1 | 8 | 9 | 8 | 5 | 8 | 8 | 2 | 8 | 1 | 1 | 1 | 2 |
| 20 | FKBP8 | 9 | 7 | 3 | 5 | 9 | 4 | 5 | 1 | 5 | 3 | 3 | 5 | 7 | 7 | 3 | 7 | 4 | 5 | 3 | 4 |
| 21 | TRAF1 | 8 | 1 | 1 | 8 | 7 | 2 | 1 | 8 | 8 | 2 | 1 | 5 | 8 | 8 | 2 | 8 | 1 | 1 | 2 | 2 |
| 22 | DRAP1 | 8 | 1 | 2 | 8 | 8 | 1 | 1 | 1 | 8 | 1 | 9 | 5 | 8 | 8 | 2 | 8 | 1 | 1 | 1 | 1 |
| 23 | ZNF148 | 1 | 1 | 1 | 8 | 1 | 1 | 1 | 1 | 1 | 8 | 1 | 7 | 1 | 2 | 1 | 1 | 8 | 8 | 1 | 1 |
| 24 | TP53BP2 | 1 | 8 | 2 | 8 | 2 | 9 | 1 | 8 | 9 | 1 | 8 | 3 | 8 | 9 | 2 | 1 | 9 | 8 | 1 | 2 |
| 25 | H326 | 6 | 4 | 8 | 9 | 9 | 1 | 8 | 4 | 7 | 7 | 7 | 5 | 6 | 5 | 9 | 9 | 5 | 7 | 3 | 4 |
| 26 | SCAMP3 | 1 | 1 | 1 | 8 | 8 | 1 | 1 | 1 | 8 | 2 | 8 | 1 | 9 | 9 | 1 | 8 | 1 | 1 | 1 | 2 |
| 27 | PDK2 | 5 | 5 | 5 | 5 | 4 | 7 | 5 | 9 | 5 | 4 | 5 | 5 | 5 | 5 | 4 | 5 | 7 | 5 | 5 | 4 |
| 28 | ELF1 | 9 | 3 | 9 | 8 | 9 | 1 | 2 | 1 | 8 | 2 | 1 | 5 | 8 | 2 | 1 | 3 | 1 | 1 | 9 | 1 |
| 29 | DCK | 8 | 2 | 3 | 8 | 8 | 9 | 8 | 1 | 8 | 9 | 1 | 5 | 8 | 1 | 1 | 9 | 8 | 8 | 1 | 8 |
| 30 | SSR1 | 8 | 9 | 3 | 8 | 1 | 9 | 1 | 9 | 9 | 8 | 1 | 5 | 9 | 9 | 2 | 9 | 1 | 8 | 1 | 9 |
| 4740 | EIF3S5 | 2 | 1 | 8 | 7 | 3 | 8 | 8 | 1 | 3 | 1 | 3 | 5 | 3 | 3 | 3 | 4 | 1 | 1 | 3 | 1 |

**Table 2.** Mechanism-based table for each of 20 doxorubicin-induced breast cancer patients by open reading frame (ORF).

**Planckian Distribution Equation (PDE)-based analysis of mRNA data:**

Derived from the planck-shannon classifier in 2008, PDE is an algorithm that can map three or more sets of long-tailed histograms (LAH's) into one or more categories of functions, each category exhibiting a linearly correlated line on the Planckian plane (Ji, 2008). PDE is based on Planck's equation for the wavelength and intensity of blackbody radiation (see **Figure 5a**) and has proven to be a successful, novel quantitative method to determine potential drug targets (Ji, 2018; Ji, 2008). Its use in making statistically valid scientific inferences within medical applications has been widely studied and verified in the past (Ji, 2015).

PDE's (see **figure 5b)** derivation from the *blackbody radiation-like equation* replaces the universal constants and temperature with free parameters, A, B and C, resulting in the algorithm $y = (A/(x + B)^5)/(e^{C/(x + B)} - 1)$, where x is unspecified and y represents the cellular wave-frequency. Within PDE, the transformed a-parameter represents the number of standing waves per unit frequency per unit volume of the cell, while the c-parameter indicates the average energy of each wave (Ji, 2018). PDE can also be derived from the Gaussian-like equation (GLE), $y = Ae^{-(x-\mu)^2/2\sigma^2}$ (where A is a parameter unrelated to A appearing in PDE), by non-linearly transforming its independent variable, x, and keeping the dependent variable y constant (Ji, 2018, p. 357). The possible reasons for the universality of PDE (i.e., PDE fits almost any long-tailed histograms generated in almost all fields of inquiry) include (i) the universality of the wave-particle duality, (ii) selection of subsets of random processes as the basic mechanism of generating order, organization, and structure in the Universe, and (iii) the Planckian process as active symmetry-breaking process driving the self-organization of the Universe (Ji, 2015; Ji, 2016).  In PDE (see **figure 1b**), the first term is known (in analogy to the blackbody radiation equation) to be related to the number of vibrational modes per unit frequency of volume and the second term is known to be related to the average energy of each mode (Nave, 2020). PDE has

been found to fit a wide-range of long-tailed histograms within biochemistry, such as that seen in Panels c) and d) in **Figure 5**. By having flexible parametric values A, B, and C, single point residual values of the PDE curve relative to the experimental curve can be easily decreased to allow PDE to better fit the curve.

PDE has been proven to be biologically viable in differentiating between sequential genomic data within breast cancer patients and placebos in the past, but this study represents its first use on a complete transcriptome to predict the efficacy of treatment (Ji, 2019). Our study equipped PDE by first compiling the data of the 20 breast cancer patients into a single location, specifically listing the cellular mRNA levels of each of 4,704 genes pre and post-doxorubicin treatment and the associated treatment *mechanism* (see above) of each open reading frame (ORF). We then studied the ORFs for each mechanism of each patient by first dividing the overall mRNA transcriptome into 10 individual datasets split between 5 short-surviving (patients surviving under 10 months) and 5 long-surviving (patients surviving greater than 75 months). Histograms were developed for each dataset of each patient (each representing one of 9 studied mechanisms for the selected patient) using a bin range of 0-5.0 at intervals of 0.1 to include all data within 3 standard deviations (σ) of the respective mean (μ). The bin range and intervals were chosen based on prior PDE-analysis from Ji (2008; 2012). For each histogram, the x-axis represents the bin number and the y-axis represents the mRNA levels within a given bin range. The experimental curve for the 9  mechanisms of each patient for the before data was fitted by the PDE until all residual values were minimized. PDE was implemented in single steps for each term of the algorithm (A, B, and C) and then combined, to minimize errors within the study. The single steps were then combined, and the residual sum of squares (RSS) between the PDE value and experimental function value for each ORF was calculated. Solver Software was then used to

minimize this value, thereby accurately fitting the PDE curve to the experimentally generated

curve. **Figure 5d**) displays the results of fitting mRNA histogram to the PDE curve for before

data of a short surviving patient - Patient 12 - over 100 ORF's.

Similar histogramical PDE analysis was conducted for the after (AF) doxorubicin mRNA

data in relation to specific mechanisms. After fitting the PDE to each mechanism for each

patient, A and C data pairs were compiled for both the before and after data. The parameter A

values were then transformed to their logarithms in order to represent them on the same scale as

C, which is defined as an exponential term in PDE.  Thus, a given (A, C) pair was converted to

an equivalent  (log(A), C) pair.

The (A', C) points for the 5 short-surviving points and the 5 long-surviving points for

each mechanism were utilized to create 20 linear regression models, inclusive of both before and

after data. Examples of a single model for each before and after dataset is shown in **figures 5e**

and **5f**. Change in slope was then calculated for each linear regression model ($\Delta M = mAF -$

mBE), and a final plot was developed where the x-coordinates represented the mechanism value

and the Y coordinates displayed the $\Delta M$ value for said mechanism. These drug-induced $\Delta M$

generated 2 values for each mechanism: one representing the drug-induced change for long-

surviving patients and one representing the drug-induced change for short-surviving patients.

| a) | b)  Planckian Distribution Equation (PDE): $$y = A/(x + B)^5/(e^{C/(x + B)} - 1)$$ |
|---|---|

## Plank's Equation

$$B_\lambda = \frac{2hc^2}{\lambda^5} \frac{1}{\exp\frac{hc}{\lambda kT} - 1}$$

Where:

$B_\lambda$ = Magnitude of Radiation per Wavelength.

$\lambda$ = Wavelength.

$h$ = Plank's Constant ($6.6238 * 10^{-34}$ Js).

$c$ = Speed of Light ($3.0 * 10^8$ m/s).
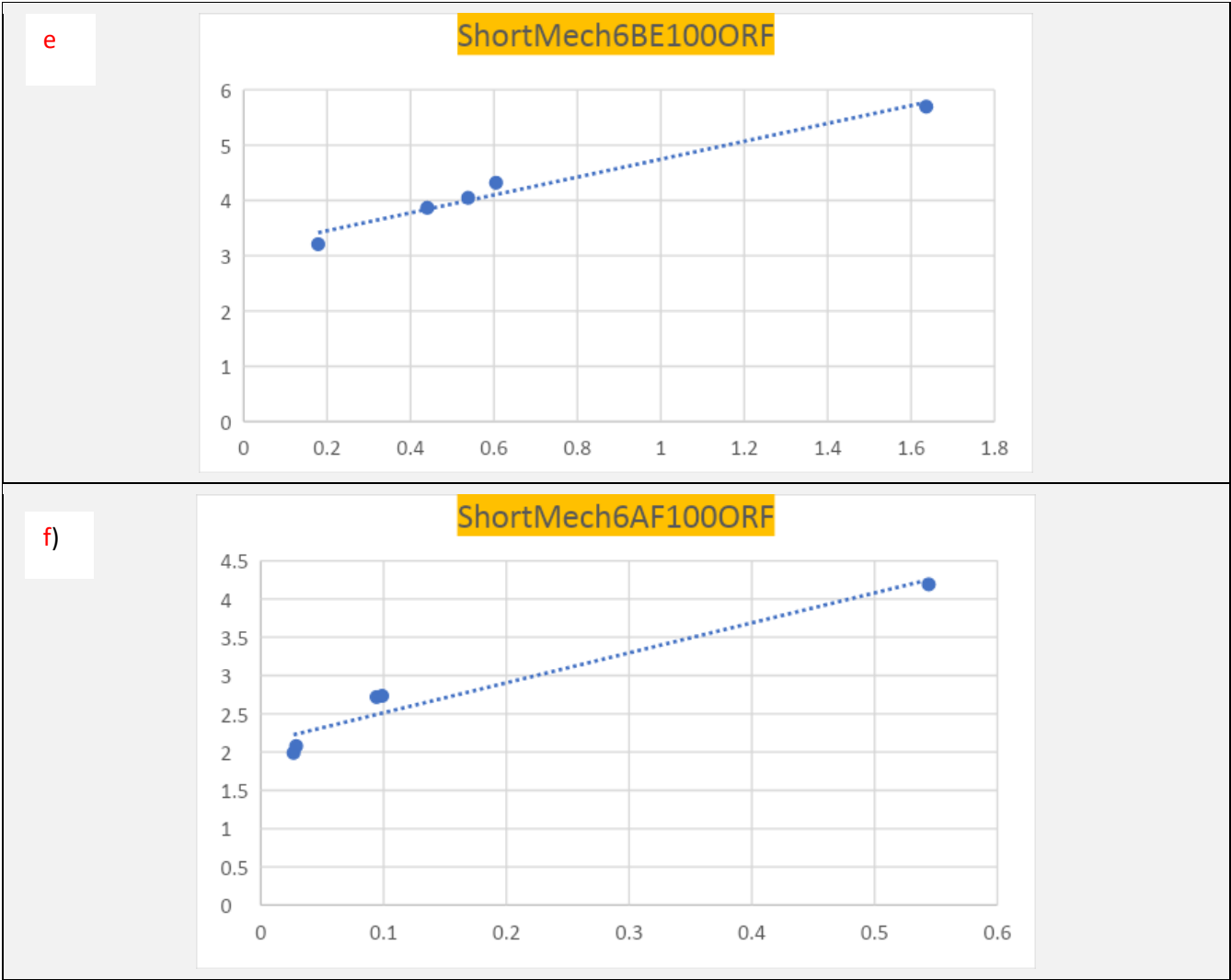
$k$ = Boltzmann Constant ($1.3807 * 10^{-23}$ J/K).

c)

**Single-molecule cholesterol oxidase turnover time histogram fit to the Planckian distribution**
A = $1.5\times10^{13}$, B = 24, C = 309.7, RMSD = 14.80 by Solver
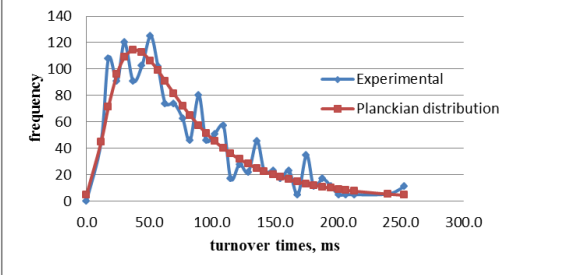
d)

Short Patient 12, 100 ORF BE; A= 0.604989, B = 0, C = 4.31865
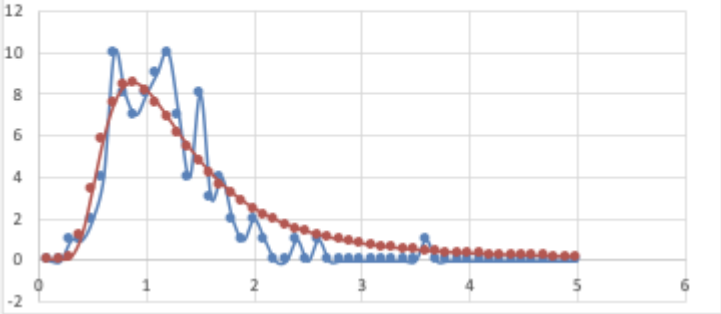
**Figure 5.** The origin and applications of the Planckian Distribution Equation (PDE).
Panel a) Planck's blackbody equation developed for quantum mechanics and wavelength/frequency/energy comparison.

Panel b) Planckian Distribution Equation (also called Blackbody Radiation-like Equation, BRE) was derived from the Planck's radiation formula (PRF) by replacing the universal constants and temperature in PRF with free parameters, A, B and C (O'Brien et al., 2006). The interpretation of the two terms given above is adopted from the interpretation of the similar terms in Planck's blackbody radiation equation (see a))

Panel c) Example use of PDE to fit to experimental data represented as a long-tailed histogram.; visual interpretation shows theoretical curve mimicking the experimental curve in extremely similar fashion.

Panel d) Example use of PDE to fit experimental breast cancer data of 67 open reading frames; panel displays relative A, B, C values from the PDE curve implemented within the algorithm to fit experimental data.

Panel e) (A', C) plot for mechanism 6 short patients with use of the **before** data; analysis is conducted for 100 open reading frames of the transcriptome

Panel f) (A', C) plot for mechanism 6 short patients with use of the **after** data; analysis is conducted for 100 open reading frames of the transcriptome

## Results and Discussions:

The logA vs. C plots for each of the 9 mechanisms long-surviving and short-surviving before and after drug treatment produced the results summarized in **Table 3**. As shown in column 4, each plot displayed a statistically significant relationship between the two variables ($R^2 > 0.700$). The results for the change in slope of the plots for each mechanism is defined by a single value in **Table 3** (see the column 6), which displays the difference in drug-induced mRNA change between long and short surviving patients.

**Table 3** indicates that the average standing energy of a standing cellular wave is greater among long-surviving patients than short-surviving patients in mechanisms 1, 2, 3, 4, 6, and 8 post-treatment. Excluded mechanisms 5 and 9 represent a decrease in tumor mRNA levels with no drug-induced mRNA change and no significant change in mRNA expression, respectively. Since neither displays a conclusive relationship about drug-induced change, mechanisms 5 and 9 are biochemically insignificant for patient treatment. Hence, the study can conclude that doxorubicin-induced slope changes were significantly greater among long-surviving breast cancer patients than short-surviving breast cancer patients for each remaining mechanism.

**Table 3.** Drug-induced changes in the slopes of the Log(A) vs C plots of the human breast cancer RNA levels exhibiting Mechanisms 1, 2, 3, 4, 5, 6, 7, 8, or 9. A and C are two of the three parameters of Planckian Distribution Equation (PDE), $y = (A/(x + B) 5)/(e^{C/(x + B)} – 1)$.

| Mechanisms | Longevity | ΔSlope | $R^2$ | ΔSlope = Slope$_{AF}$ – Slope$_{BE}$ | ΔSlope = ΔSlope$_{Long}$ – ΔSlope$_{Short}$ |
|---|---|---|---|---|---|
| **1** | Short AF | 1.0354 | 0.986 | -0.1136 | |

|  | Short BE | 1.149 | 0.984 |  | 0.011 |
|  | Long AF | 0.8933 | 0.989 | -0.1026 |  |
|  | Long BE | 0.9959 | 0.996 |  |  |
| 2 | Short AF | 1.0028 | 0.908 | 0.1304 |  |
|  | Short BE | 0.8724 | 0.973 |  | 0.2404 |
|  | Long AF | 1.2181 | 0.97 | 0.3708 |  |
|  | Long BE | 0.8473 | 0.947 |  |  |
| 3 | Short AF | 1.0424 | 0.963 | 0.3982 |  |
|  | Short BE | 0.6442 | 0.981 |  | 0.2042 |
|  | Long AF | 1.3782 | 0.992 | 0.6024 |  |
|  | Long BE | 0.7758 | 0.972 |  |  |
| 4 | Short AF | 0.7842 | 0.997 | 0.323 |  |
|  | Short BE | 0.4612 | 0.996 |  | 0.1091 |
|  | Long AF | 0.8815 | 0.996 | 0.4321 |  |
|  | Long BE | 0.4494 | 0.982 |  |  |
| 5 | Short AF | 0.5625 | 0.994 | 0.0032 |  |
|  | Short BE | 0.5593 | 0.997 |  | -0.0487 |
|  | Long AF | 0.4150 | 0.99 | -0.0455 |  |
|  | Long BE | 0.4605 | 0.992 |  |  |
| 6 | Short AF | 0.495 | 0.983 | -0.2904 |  |
|  | Short BE | 0.7854 | 0.9564 |  | 0.0655 |
|  | Long AF | 0.5265 | 0.9855 | -0.2239 |  |
|  | Long BE | 0.7504 | 0.9317 |  |  |
| 7 | Short AF | 0.6283 | 0.9267 | -0.1935 |  |
|  | Short BE | 0.8218 | 0.64 |  | -0.1378 |
|  | Long AF | 1.183 | 0.978 | -0.3673 |  |
|  | Long BE | 1.5503 | 0.773 |  |  |

| 8 | Short AF | 0.7401 | 0.9943 | -0.4114 | |
| | Short BE | 1.1515 | 0.972 | | 0.0288 |
| | Long AF | 0.6245 | 0.9915 | -0.3826 | |
| | Long BE | 1.0071 | 0.982 | | |
| 9 | Short AF | 0.7638 | 0.99 | -0.0009 | |
| | Short BE | 0.7647 | 0.978 | | -0.1007 |
| | Long AF | 0.6631 | 0.904 | -0.1016 | |
| | Long BE | 0.7647 | 0.978 | | |

A final plot seen in **Figure 6** summarizes the results of the present study. Mechanism values 1-9 are ordered on the x-axes and drug-induced changes in slope between long-surviving and short-surviving patients are presented on the y-axes. The results display a wave-like distribution for slope changes as a function of each mechanism, which can be used as evidence for the anti-cancer efficacy of other drug candidates. This procedure is described in more detail in **Table 4**, which displays the process by which treatment longevity can be predicted. Studies should biopsy breast cancer tissue before drug treatment, then cell culture said tissue in the presence and absence of the drug candidate to generate the AF and BE data. Analysis should then be conducted as illustrated in this paper by (1) measuring the genomic mRNA levels in BE and AF tissue samples with genome-wide cDNA microarrays, (2) determining the values of the A and C parameters, and (3) plotting log A vs. C for both BE and AF data. The drug-induced changes in the slopes of the regression line of log A vs. C plots must be computed for each mechanism and a chart similar to that presented in **Table 7b** must be developed. By visual examination of the curve distribution for the mechanism vs. drug-induced slope change of long and short survivors plot, the drug-candidate that best mimics doxorubicin and proves to be an effective therapeutic can be identified. Algorithmic computation can also be done by determining

which therapeutic candidate best mimics the doxorubicin plot via calculation of the residual ($\hat{y}^2$)

for each mechanism. The drug candidate that presents the lowest value for the residual sum of

squares (RSS) represents the most effective anticancer therapeutic.



**Figure 6:** Complete chart displaying the difference in drug-induced changes (y-axis) in slope of the log A vs. C plots between long and short surviving patients for each mechanism (x-axis
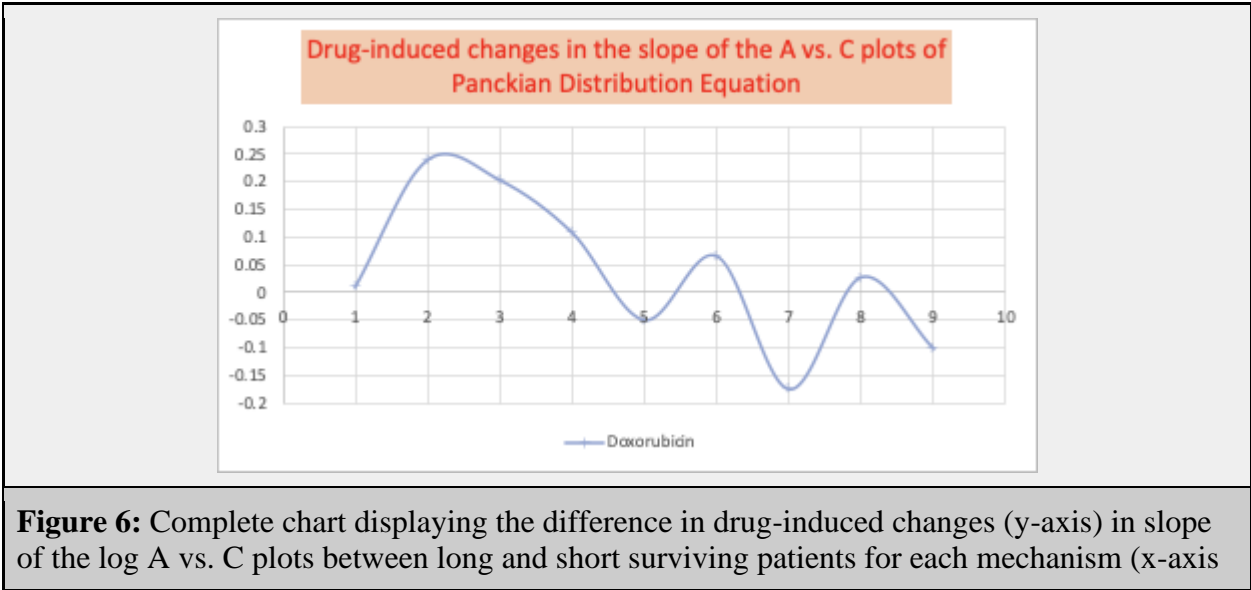
1) Biopsy the tumor and normal breast tissue before drug treatment.

2) Cell culture the biopsied tissues in the presence (or AFter) or absence of (or BEfore) the anticancer drug.

3) Measure the RNA levels in BE and AF tissue samples with genome-wide cDNA microarrays.

4) Determine the A and C parameter values of the Planck Distribution Equation fitting the BE and AF data.

5) Construct the log A vs C plots.

6) Compute the drug-induced changes in the slopes of the regression lines of the log A vs C plots.

**Table 4**. Procedures for obtaining mRNA data forPDE-based analysis  to discover doxorubicin-like drugs mimicking the wave-like curves depicted in Figure 6.

**Figure 7** displays a hypothetical scenario that predicts which of 5 drug candidates will

prove most effective in treating breast-cancer. The scenario displays use of both the method of

visual examination (7a) and the method of RSS numerical comparison (7b). As presented in the

results of the scenario, use of either method yields the same result - hypothetical candidate 3 (Ji,

2018). Through determining which drug most mimics the patient survival-outcome of proven

treatment Doxorubicin, the scenario was potentially able to identify the most effective candidate.
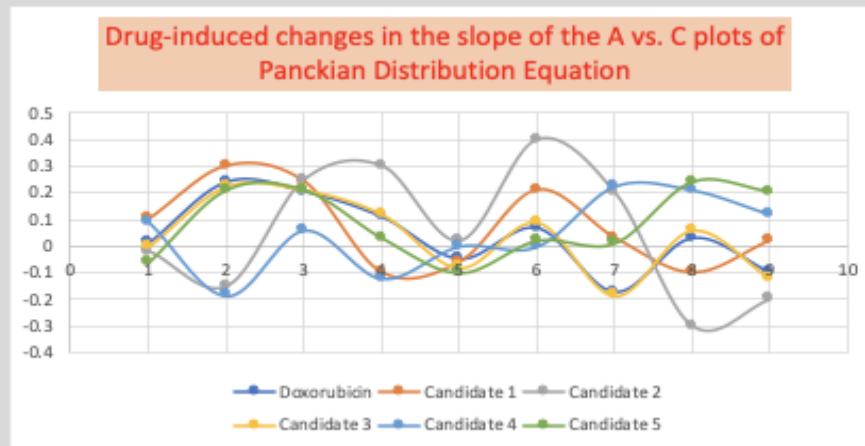
Drug candidates that do not mimic Doxirubison's behavior can be interpreted to be suboptimal

treatment methods since they produce results that do not maximize patient-survival in each

mechanism. Additional 2sample hypothesis tests can be conducted using an alpha level of 0.05 to

determine which therapies, if any, significantly differ from the others.

a)



b)

| Mech # | Doxo-rubicin | Drug1 | $\Delta^2(1)$ | Drug2 | $\Delta^2(2)$ | Drug3 | $\Delta^2(3)$ | Drug4 | $\Delta^2(4)$ | Drug5 | $\Delta^2(5)$ |
|---|---|---|---|---|---|---|---|---|---|---|---|
| 1 | 0.011 | 0.102 | 0.00828 | -0.02 | 0.00096 | 0 | 0.00012 | 0.09 | 0.00624 | -0.06 | 0.00504 |
| 2 | 0.2404 | 0.3 | 0.00355 | -0.15 | 0.15241 | 0.225 | 0.00023 | -0.185 | 0.18096 | 0.21 | 0.00092 |
| 3 | 0.2042 | 0.24 | 0.00128 | 0.25 | 0.00209 | 0.211 | 0.00004 | 0.06 | 0.02079 | 0.21 | 0.00003 |
| 4 | 0.1091 | -0.1 | 0.04372 | 0.3 | 0.03644 | 0.12 | 0.00011 | -0.12 | 0.05248 | 0.03 | 0.00625 |
| 5 | -0.0487 | -0.06 | 0.00012 | 0.02 | 0.00471 | -0.08 | 0.00097 | 0 | 0.00237 | -0.1 | 0.00263 |
| 6 | 0.0665 | 0.21 | 0.02059 | 0.4 | 0.11122 | 0.09 | 0.00055 | 0 | 0.00442 | 0.02 | 0.00216 |
| 7 | -0.1738 | 0.03 | 0.04153 | 0.2 | 0.13972 | -0.185 | 0.00012 | 0.225 | 0.15904 | 0.011 | 0.03415 |
| 8 | 0.0288 | -0.1 | 0.01658 | -0.3 | 0.10810 | 0.06 | 0.00097 | 0.211 | 0.03319 | 0.2404 | 0.04477 |
| 9 | -0.1007 | 0.02 | 0.01456 | -0.2 | 0.00986 | -0.12 | 0.00037 | 0.12 | 0.04870 | 0.2042 | 0.09296 |
| Sum of $\Delta^2$ | | | 0.15024 | | 0.56555 | | **0.00352** | | 0.50822 | | 0.18893 |

A new Doxorubicin-like drug

**Figure 7.** Example of a hypothetical analysis of mRNA levels for discovering new anticancer drugs.  Δ = Slope of the log A vs. C plot (candidate drug) – Slope of the log A vs. C plot (doxorubicin).

Panel a) Displays plot of drug-induced changes in the slope of logA vs C plots of PDE for each of the 5 drug candidates relative to doxorubicin. Drug candidate 3's curve nearly mimics the doxorubicin curve; hence drug candidae 3 is most likely the best anti-breast cancer drug of the 5 drug candidates.

Panel b) Displays raw data table for each drug candidates' changes in the slope of the log A vs C plots of PDE. Includes residual between drug-induced change and doxorubicin change and RSS for each therapeutic. Drug 3 displays the lowest sum of residual squares and is thus the most effective drug. Additional 2sample t-tests can be conducted using an alpha level of 0.05 to determine which therapies, if any, significantly differ from the others.

### Conclusions:

Research has shown that chemotherapy has caused or hastened death in more than 27% breast cancer patients, a direct result of improper pharmacotherapy (Megget, 2008). The purpose of this novel study is to provide an effective method of predetermining the efficacy of breast cancer pharmacotherapy.

To do so, we hypothesized that using the Planckian Distribution Equation (PDE) discovered at Rutgers University would allow for us to develop a novel predictive procedure for anticancer drugs (Ji, 2018). PDE has become a common medical research tool as a result of its ability to fit nearly all long-tailed histograms (Ji, 2008). We analyzed the mRNA data (rather than the mRNA nucleotide sequence data) measured from 20 breast cancer patients using the PDE-derived log A vs. C plots (Perou et al., 2000). The mRNA genome was compiled using advanced microarray data collection on tumor tissue before (BE) and after (AF) doxorubicin treatment for 16 weeks. PDE-fitted linear regression models were then developed for each data subset derived from the free-parameters A and C, where X represented Log(A*10^3) and Y represents C. A second subset of this data was developed such that the mechanism value was represented by the X-coordinates and the net difference in slope change between long and short-surviving patients ($\Delta M_2 = \Delta M_{Long} - \Delta M_{short}$) was represented by the Y-axis. Each plot

demonstrated a high correlation between the two variables ($R^2 > 0.70$). The final model displays each mechanism along the X axis and a wave-like distribution of the mean difference between long and short surviving patients along the Y axis.

By following the procedure defined in **Table 4**, potential anti-breast cancer drugs can be efficiently identified. Visual or quantitative comparison of a drug-candidate's generated plot to that of the doxorubicin plot provides a novel method to predict the clinical efficacy of the breast-cancer therapeutic.

It is important, however, to ensure that this research does not end with the results of this single PDE based analysis. We have provided a novel biostatistical skeleton for analysis of independent breast-cancer transcriptomes. We hope, though, that future studies will confirm and refine our methodology about the use of the Planckian Distribution Equation-based algorithms described in this paper as an effective strategy for discovering novel anti-cancer drugs. Just as prominent cancer research figures Sidney Farber and Mary Lasker would echo, *the war on cancer* is just that; a never ending battle defined not by a single victory, but by small progression towards early detection and curing (Mukherjee, 2010).

## References:

Rashbass, J. (2016, August 31). Chemotherapy is powerful stuff but data is too. Retrieved

September 26, 2020, from

https://publichealthmatters.blog.gov.uk/2016/08/31/chemotherapy-is-powerful-stuff-but-

data-is-too/

Ji, S. (2008). Modeling the single-molecule enzyme kinetics of cholesterol oxidase based

on Planck's radiation formula and the principle of enthalpy-entropy compensation, in

Short Talk Abstracts,  The 100th Statistical Mechanics Conference, December 13-16,

Rutgers University, Piscataway, N.J

Ji, S. (2012).  Molecular Theory of the Living Cell: Concepts, Molecular Mechanisms,

and Biomedical Applications. Springer, New York.  Pp. 193-195.

Center, J. (2020, January 13). Top Five Most Dangerous Cancers in Men and Women.

Retrieved September 26, 2020, from https://www.unitypoint.org/desmoines/services-

cancer-article.aspx?id=c9f17977-9947-4b66-9c0f-15076e987a5d

O'brien, M. E., Borthwick, A., Rigg, A., Leary, A., Assersohn, L., Last, K., . . . Smith, I.

E. (2006). Mortality within 30 days of chemotherapy: A clinical governance

benchmarking issue for oncology patients. *British Journal of Cancer, 95*(12), 1632-1636.

doi:10.1038/sj.bjc.6603498

Perou, C. M., Sorlie, T., Eisen, M. B*., et al.* (2000). Molecular portraits of human breast

tumors.  *Nature* 406(6797): 747-52.

Perou, C. M., Jeffrey,  S. S., van de Rijn, M*., et al.* (1999).  Distinctive gene expression

patterns in human mammary epithelial cells and breast cancers. *Proc. Natl. Acad. Sci.*

*USA*

Grigoryev W., Ahmad M., KMC, Dr Amanda Welch on October 11, Welch, D., O, A., . . . Jacklyn. (2020, April 02). Introduction to DNA Microarrays. Retrieved September 26, 2020, from https://bitesizebio.com/7206/introduction-to-dna-microarrays/

Ji, S., Chaovalitwongse, A., Fefferman, N., Yoo, W. & Perez-Ortin, J. E. (2009). Mechanism-based Clustering of Genome-wide mRNA Levels: Roles of Transcription and Transcript-Degradation Rates.  In: *Clustering Challenges in Biological Networks*, S. Butenko, A. Chaovalitwongse, and P. Pardalos, (eds.), World Scientific Publishing Co., Singapore, pp. 237-255.

Ji, S. (2012).  Morphogenesis of Drosophila melanogaster.  In: *Molecular Theory of the Living Cell: Concepts, Molecular Mechanisms, and Biomedical Applications*. Springer, New York.  Section 15.1, pp. 521-547.  Available at conformon.net under Publications > Book Chapter.

Ji, S. (2012).  Principles of Self-Organization and Dissipative Structures.   In [1], Section 3.1, pp. 69-78.

Ji, S. (2012).  Ribonoscopy and Theragnostics.  In [1],   Chapter 19, pp. 607-620.

Perou, C. M., Sorlie, T., Eisen, M. B*., et al.* (2000).  Molecular portraits of human breast Tumors. *Nature* 406(6797): 747-52.

Ji, S. (2018). Mathematical (Quantitative) and Cell Linguistic (Qualitative) Evidence for Hypermetabolic Pathways as Potential Drug Targets.  *J. Mol. Gene. Med.* **12** (2): 1000343.

Ji, S. (2015). Planckian distributions in molecular machines, living cells, and brains: The wave-particle duality in biomedical sciences.  In: P*roceedings of the International*

*Conference on Biology and Biomedical Engineering,* Vienna, March 15-17, 2015. Pp. 115-137.

Ji, S. (2016). WAVE-PARTICLE DUALITY IN PHYSICS AND BIOMEDICAL SCIENCES.

Ji, S. (2018). *The Cell Language Theory: Connecting Mind and Matter.* World Scientific Publishing, New Jersey (Ch7).

Megget, K. (2008, November 13). Chemotherapy causes death in more than 25% of cancer patients. Retrieved September 26, 2020, from

http://www.pharmatimes.com/news/chemotherapy_causes_death_in_more_than_25_of_cancer_patients_986391

Nave, R. (2020). Blackbody Radiation. Retrieved October 15, 2020, from:

http://hyperphysics.phy-astr.gsu.edu/hbase/mod6.html

Mukherjee, S. (2010). *The emperor of all maladies: A biography of cancer*. New York: Scribner

Ji, S. (2015). Planckian Information (Ip): A New Measure of Order in Atoms, Enzymes, Cells, Brains, Human Societies, and the Cosmos. Unified Field Mechanics. doi:10.1142/9789814719063_0062

Ji, S., Park, B. J., &amp; Reid, J. S. (2019). Planck–Shannon Classifier: A Novel Method to Discriminate Between Sonified Raman Signals from Cancer and Healthy Cells. Advances in Artificial Systems for Medicine and Education II Advances in Intelligent Systems and Computing, 185-195. doi:10.1007/978-3-030-12082-5_17